Available online at www.sciencedirect.com
SCIENCE DIRECT
Journal of Sound and Vibration 295 (2006) 708–724
JOURNAL OF SOUND AND VIBRATION
www.elsevier.com/locate/jsvi

A tunable electromagnetic vibration absorber: Characterization and application

Jie Liu, Kefu Liu*

Department of Mechanical Engineering, Lakehead University, 955 Oliver Road, Thunder Bay, Ont., Canada P7B 5E1

Received 2 February 2005; received in revised form 22 December 2005; accepted 17 January 2006
Available online 11 April 2006

Abstract

The paper presents a newly designed electromagnetic vibration absorber (EMVA), whose stiffness is on-line tunable. The EMVA is capable of suppressing vibration of the primary system excited by a harmonic force with a variable frequency. The EMVA consists of a clamped–clamped aluminum beam and a permanent magnet that is embedded in the center of the beam and placed between two poles of a C-shaped electromagnet. By varying the current of the electromagnet, stiffness of the EMVA can be adjusted instantaneously such that the absorber frequency can be tuned. A detailed characterization of the EMVA is presented. The effective stiffness of the absorber is determined numerically and validated experimentally. To test its effectiveness in vibration suppression, the EMVA is used to track two types of the exciting frequency variations: multi-step and linear. The response of the absorber mass is used to tune the EMVA to ensure that the absorber frequency equals the exciting frequency.

1. Introduction

Tunable vibration absorbers belong to the family of semi-active control systems. Semi-active control systems are attracting more research interest in the field of vibration control, since they combine the advantages of both passive and active control systems. On one hand, they preserve the reliability of the passive control systems even in the event of power loss; on the other hand, they possess the versatility and adaptability of the active systems without a great amount of power consumption. Generally, the mechanical properties of the semi-active systems, such as the stiffness and/or the damping value, can be adjusted based on the feedback from the measured response and/or the excitation. Several variable stiffness vibration absorbers have been proposed. Stiffness variation of the device reported in Ref. [1] was achieved by varying the effective number of coils in a helical spring used as the absorber stiffness. The same vibration absorber was used to study non-collocated adaptive-passive vibration control in Ref. [2]. A vibration absorber developed in Ref. [3] consists of a flexible cantilever beam attached by a mass at its free end. By varying the length of the beam, the absorber frequency can be varied. A variable stiffness device proposed in Ref. [4] has four coil springs arranged in a plane rhombus configuration. The aspect ratio of the rhombus configuration can be varied by a linear

*Corresponding author. Tel.: +1 807 343 8634; fax: +1 807 343 8928.
E-mail address: kefu.liu@lakeheadu.ca (K. Liu).

0022-460X/$ - see front matter © 2006 Elsevier Ltd. All rights reserved.
doi:10.1016/j.jsv.2006.01.033

electromechanical actuator to achieve a continuous variation of the absorber stiffness. In Ref. [5] a variable stiffness absorber similar to the one developed in Ref. [3] was used to compare two different tuning algorithms. It is noted that all the above tunable devices involve an electro-mechanically driven system. As a result, a slow reaction speed may become the main concern for these types of stiffness control devices. Alternatively, damping is sometimes added to the absorber systems to improve the effective bandwidth of operation. Damping value can be made on-line adjustable by utilizing a variable-orifice valve to alter the resistance to the flow of a conventional hydraulic fluid damper [6,7]. Friction dampers have also been widely studied as another approach in semi-active vibration control [8,9]. Most noticeably, electro-rheological or magneto-rheological dampers feature a broad-bandwidth modulation of the damping characteristics through the variation of an electrical or magnetic field [10–12]. However, when adding the damping into the system, the performance of the absorber at the design frequency is sacrificed.

Over the past decade, various devices based on magnetism or electromagnetism have been used to suppress vibration. The electromagnetic servomechanism developed in Ref. [13] consists of two paired electromagnets and permanent magnets. When the electromagnets are energized, interacting forces are produced between the paired electromagnets and permanent magnets. The device was used in the study of active vibration control. In Ref. [14] permanent magnets were used to build an extremely soft spring for the purpose of vibration isolation. A hybrid-type active vibration isolation system developed in Ref. [15] uses both electromagnetic and pneumatic forces. In Ref. [16] an electromagnetic device was designed to parametrically excite the experimental beam. The phenomenon of eddy current has been explored to develop magnetic dampers [17–19].

This paper presents a newly designed electromagnetic vibration absorber (EMVA). Similar to the devices reported in Refs. [1–5] the device developed in this study is a variable stiffness one. However, a notable difference is that the present device is non-contact, with non-mechanical motion, and the stiffness can be changed instantly. Also, different from the electromagnetic devices referred above, the present system is tunable on-line. It should be noted that in Refs. [13–16] approximate approaches were employed to establish the electromagnetic interaction. An extensive literature search has indicated that a method to quantify the stiffness characteristics of the EMVA is not readily available. The detailed stiffness characterization presented in this study is useful for the design of similar devices.

The following sections of the paper are organized as follows: In Section 2, the developed EMVA is introduced and an experimental setup used to test the EMVA is explained. In Section 3, characterization of the EMVA is presented. In Section 4, an experimental calibration is conducted and the performance of the EMVA is tested. In Section 5, the conclusions of the study are given.

2. Electromagnetic vibration absorber

Fig. 1 shows a photograph of the developed electromagnetic vibration absorber attached to a primary system. As shown schematically in Fig. 2, the entire experimental system consists of three subsystems: EMVA, primary system, and computer control system. The EMVA contains the following parts: a clamped–clamped aluminum beam (1), a permanent magnet (PM) (2) that is embedded in the center of the beam, and an electromagnet (3). The magnet-beam assembly is placed between the poles of the electromagnet. The electromagnet is constructed by winding Gauge 18 copper wire around a C-shaped steel core. The permanent magnet plays a dual role: acting as an absorber mass and forming a variable magnetic spring by interacting with the electromagnet through varying the direct current (DC) of the electromagnetic coils. The primary system (4) is an aluminum slab supported by an aluminum plate on each side, acting like a single degree-of-freedom (dof) system. The electromagnet is fastened to the slab by two brackets, forming part of the primary mass. A small permanent magnet (5) is glued on an aluminum bar that is clamped to the primary mass. This permanent magnet interacts with an electromagnetic shaker (6) to generate a non-contact exciting force. The purpose of adding the aluminum bar between the permanent magnet and the primary mass is to minimize the interference of the magnetic field generated by the forcing electromagnet and the magnetic field generated by the absorber electromagnet. The parameters of the system are summarized in Table 1. The computer control system is explained in Section 4.

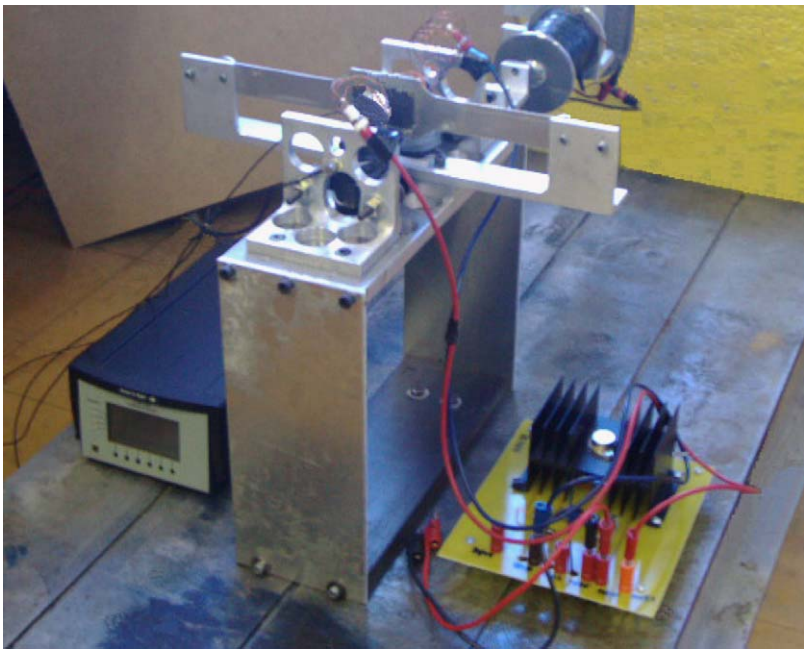

Fig. 1. Photograph of the experimental set-up.

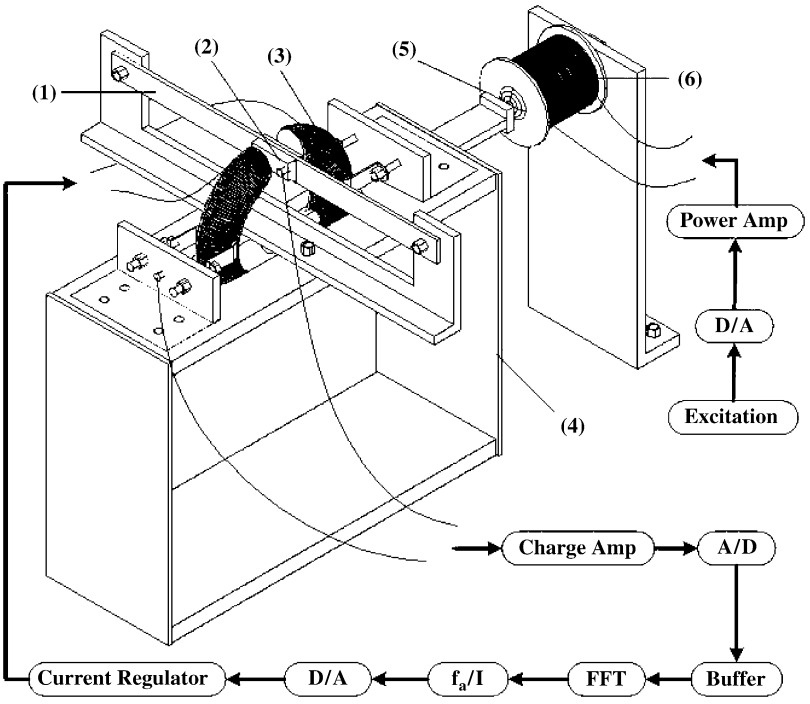

Fig. 2. Schematic of the entire experimental system.

3. Characterization of the EMVA

Characterization of the EMVA focuses on determination of the variable range of its stiffness. Such information is of importance for the design and implementation of the EMVA. Unfortunately, a systematical

Table 1
System parameters

Symbol	Description	Value
m_a	Absorber mass	0.151 kg
m	Primary mass	3.074 kg
c_a	Damping coefficient of the absorber system	0.18 Ns/m
c	Damping coefficient of the primary system	3.71 Ns/m
R_1	Inner radius of the electromagnetic coils	11 mm
R_2	Outer radius of the electromagnetic coils	20 mm
L	Circumference of the electromagnet	314.16 mm
N	Turns of the coils	784
μ_0	Permeability of free space	$4\pi \times 10^{-7}$ H/m
δ	The gap space between two pole faces of the electromagnet	42.0 mm
l	Length of the PM	48.0 mm
w	Height of the PM	22.0 mm
h	Thickness of the PM	10.0 mm

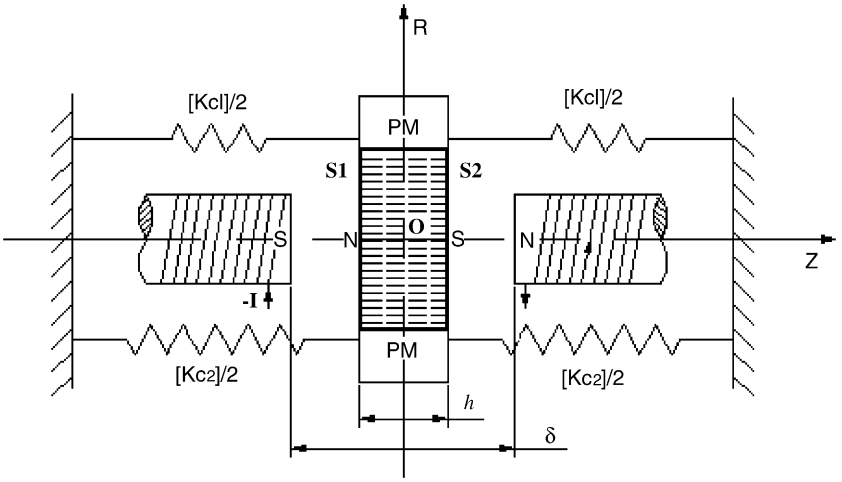

Fig. 3. Three springs involved in the EMVA.

method to calculate the stiffness of such a device has not been found in the literature. In what follows, a detailed characterization procedure is presented. It is expected that the developed approach is useful for the design of similar devices. As shown in Fig. 3, three springs are involved in the EMVA, namely, a constant spring k_{c1} created by the absorber beam, a constant spring k_{c2} due to the interaction between the PM and the core of the electromagnet, and a variable spring k_v due to the interaction between the PM and the electromagnet. To determine k_v and k_{c2}, the theory of electromagnetism is explored to obtain the relationship between the magnetic force and the displacement of the absorber mass. With this relationship, the stiffness can be established.

3.1. Magnetic stiffness due to the interaction between the electromagnet and the PM

The approach used is to first determine the interaction force between the PM and the magnetic field produced by the electromagnet. The stiffness is then equal to the derivative of the force with respect to distance. The magnetic flux density within the gap of the C-shaped electromagnet can only be determined numerically. Although a commercial finite element analysis package may be employed, this study took a different strategy. The Biot–Savart law of magnetostatics determines the constant magnetic field of an element carrying a steady current [20]. A circular current loop can be considered to be a basic element of a coil. Fig. 4

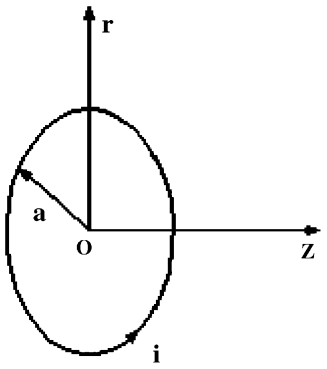

Fig. 4. Circular current loop.

shows such a loop with a radius a and current i. According to the Biot–Savart law, the magnetic flux densities at an axial distance z and a radial distance r are given as

$$B_{lr} = \frac{\mu_0 i}{2\pi}\frac{z}{r}\frac{1}{\left[(a+r)^2+z^2\right]^{1/2}}\left[E_2\frac{a^2+r^2+z^2}{(a-r)^2+z^2}-E_1\right], \tag{1}$$

$$B_{lz} = \frac{\mu_0 i}{2\pi}\frac{1}{\left[(a+r)^2+z^2\right]^{1/2}}\left[E_2\frac{a^2-r^2-z^2}{(a-r)^2+z^2}+E_1\right], \tag{2}$$

respectively, where B_{lz} is the flux density in the axial direction and B_{lr} in the radial direction, E_1 and E_2 are the complete elliptic integrals of the first and second kind, respectively, and they are of the forms

$$E_1 = \int_0^{\pi/2}\left[1-\frac{4ar}{(a+r)^2+z^2}\sin^2\theta\right]^{-1/2} \mathrm{d}\theta, \tag{3}$$

$$E_2 = \int_0^{\pi/2}\left[1-\frac{4ar}{(a+r)^2+z^2}\sin^2\theta\right]^{1/2} \mathrm{d}\theta. \tag{4}$$

The total flux densities of the electromagnet under study may be found in the following way. First, the electromagnet is considered to consist of an infinite number of such current loops. The flux densities from individual current loops are determined. Then the total flux densities are obtained by the superposition of contributions of individual loops. However, this approach proved to be more complicated than necessary. Also, the magnetic field determined would not be symmetric about the horizontal plane in the middle of the gap. Considering the fact that the size of the C-shape is relatively larger compared with the gap distance, the coil is divided into two halves in the middle of the gap and each half of the curved coil is approximated as a hollow cylinder or a solenoid with an inner radius R_1, an outer radius R_2, and a length $L/2$ where L is the circumference of the mean diameter of the coil. Without loss of generality, let us consider that the right hollow cylinder is composed of an infinite number of the circular current loops, then, the total contribution of the magnetic flux of the cylinder can be found by integrating Eqs. (1) and (2) in both the radial and axial directions:

$$B_{sr} = \int_{R_1}^{R_2}\int_0^{L/2} B_{lr}(a,r,z+\lambda)\,\mathrm{d}\lambda\,\mathrm{d}a, \tag{6}$$

$$B_{sz} = \int_{R_1}^{R_2}\int_0^{L/2} B_{lz}(a,r,z+\lambda)\,\mathrm{d}\lambda\,\mathrm{d}a, \tag{7}$$

where B_{sr} and B_{sz} are the radial and axial magnetic flux densities, respectively, with the origin located at the center of the right end face of the cylinder. Note that in the equations above, the loop current i should be

substituted by using

$$i = \frac{2NI}{(R_2 - R_1)L}, \tag{8}$$

where I is the coil current. Considering the complexity of the foregoing equations, numerical methods are commonly employed. The total magnetic flux densities can then be found by the superposition of the flux densities from the right cylinder with those from the left cylinder. The total flux density is denoted as B_{cr} and B_{cz} for the radial and axial direction, respectively. Fig. 5 shows the computed axial flux densities along the center line of the air gap.

A ferromagnetic core can significantly magnify the magnetic field produced by the coils, and such an effect is included by introducing an amplification number μ_r, which is the relative permeability of the steel core. Further, for a certain coil current, the flux available in the air gap is solely affected by the term μ_r/γ and, the denominator γ is called the leakage factor, defined as the ratio of the total flux to the gap flux. Since the value of μ_r/γ varies with materials of the core, specific experimental setups, etc., it is customary to determine it experimentally. Thus, a DC magnetometer (AlphaLab, Model: DCM) was used to measure the axial magnetic flux density at the points along the centerline of the gap of the electromagnet. Four different amplitudes of DC current were applied separately. The value μ_r/γ was determined in the following way: a modified computed axial flux density was found by multiplying a trial value μ_r/γ to the computed B_{cz}; then, the squared error between the measured axial flux density and the modified computed axial flux density was found; by varying the values of μ_r/γ the squared error was minimized. It was found that by using the value of $\mu_r/\gamma = 27.5$, minimum error resulted. Fig. 6 shows a comparison of the measured values and the computed values. Fig. 7

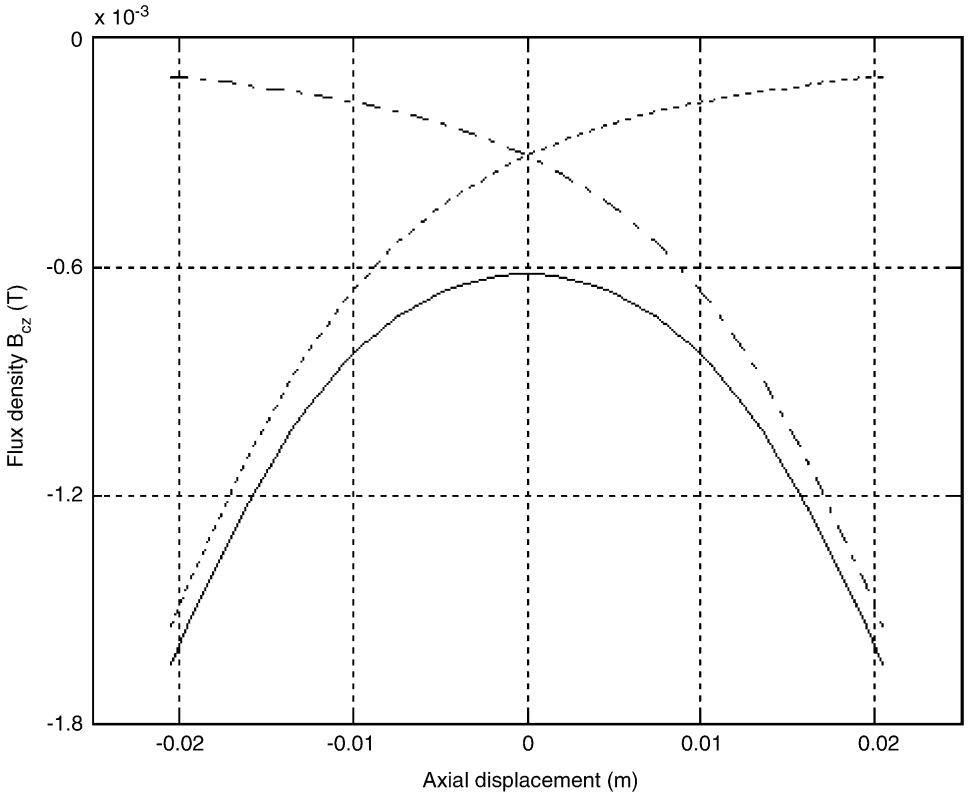

Fig. 5. Axial flux density along the centerline of the gap: dash-dot line, B_{sz} from the right cylindrical coils; dot line, B_{sz} from the left cylindrical coils; solid line, B_{cz}.

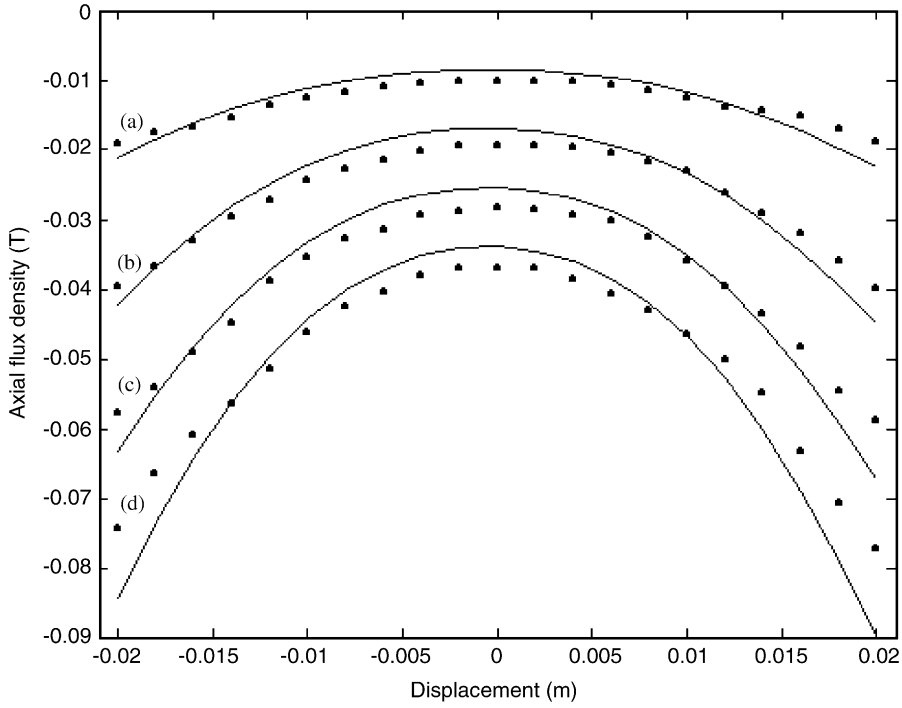

Fig. 6. Comparison of the measured values and the computed values for the axial flux density along the centerline of the gap: (a) $I = 0.5$ A, (b) $I = 1.0$ A, (c) $I = 1.5$ A, (d) $I = 2.0$ A. Dot, experimental; solid line, analytical.

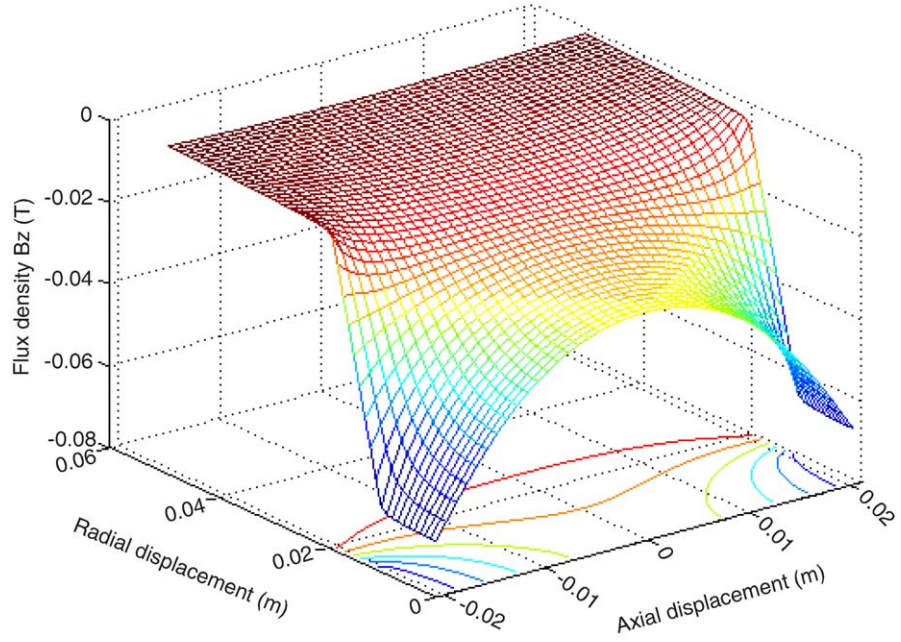

Fig. 7. The axial flux density of the electromagnet, $I = 1.5$ A.

shows a 3D plot for the axial flux density distribution when a current of 1.5 Å is applied to the electromagnet. It can be seen that the axial flux density B_z peaks along the centerline of the coils, reaches maximum on the pole faces, and becomes minimum in the middle of the air gap.

With the flux density of the electromagnet available, the interaction force between the electromagnet and the PM is given by [20]

$$F_z = -\partial W/\partial z, \tag{9}$$

where W is the energy of interaction of the electromagnet and the PM. The energy W may be calculated as the integral of the magnetization M of the PM times the potential from the electromagnet on the pole faces S_1 and S_2 of the PM (see Fig. 3). If φ_1^{em} is the potential from the electromagnet on the pole face S_1, and φ_2^{em} the potential from the electromagnet on the pole face S_2, then

$$W = \mu_0 \int_{S_1} M\varphi_1^{em}\,\mathrm{d}S + \mu_0 \int_{S_2} (-M)\varphi_2^{\mathrm{em}}\,\mathrm{d}S \tag{10}$$

or

$$F_z = -\mu_0 \int_{S_1} M\frac{\partial\varphi_1^{\mathrm{em}}}{\partial z}\,\mathrm{d}S + \mu_0 \int_{S_2} M\frac{\partial\varphi_2^{\mathrm{em}}}{\partial z}\,\mathrm{d}S = M\left(\int_{S_1} B_{z1}\,\mathrm{d}S - \int_{S_2} B_{z2}\,\mathrm{d}S\right), \tag{11}$$

where $B_{zi} = -\mu_0\partial\varphi_i^{\mathrm{em}}/\partial z$, $i = 1, 2$ is the axial flux density on the PM pole face i. Eq. (11) indicates that the force F_z is proportional to the difference between the total flux over the pole face S_1 and the total flux over the pole face S_2. Note that, due to the symmetry of distributions of the radial magnetic flux, no net interaction force exists in the radial direction. Fig. 8 shows the curves of the electromagnetic force F_z versus the displacement of the PM for four different coil currents. As shown in the figure, within the range of [−0.01, 0.01] m, the force–displacement relationship is close to linear. The linearized curves are shown in the figure as well, and their slopes (see Table 2) are the electromagnetic stiffness k_v. It should be noted that a negative stiffness is obtained by applying a negative current. As analyzed in the next section, k_{c2} is negative as well. Therefore, it is very important to design the EMVA such that $k_{c1} + k_{c2} + k_v > 0$. Also, when the displacement of the PM is too large, the nonlinearity of k_v increases significantly. In the present design, the displacement of the PM (absorber mass) is restricted not to exceed 10 mm. It is also understandable that when positive currents

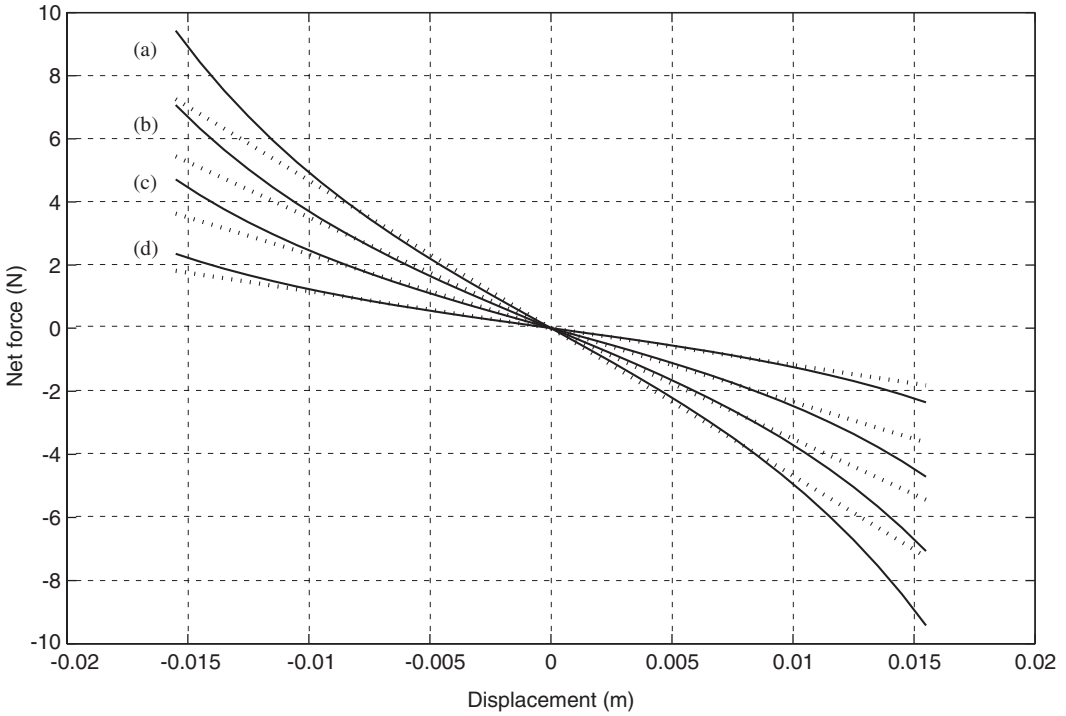

Fig. 8. Interaction force F_z versus the displacement of the PM with the origin at the gap center: (a) $I = -2.0$ A, (b) $I = -1.5$ A, (c) $I = -1.0$ A, (d) $I = -0.5$ A. Solid line, analytical; dotted line, linearized.

Table 2
Variable stiffness k_v

Coil current (A)	Analytical values (N/m)	Experimental values (N/m)	
		Loading	Unloading
−2.0	−468.15	−431.58	−416.99
−1.5	−351.10	−357.67	−327.44
−1.0	−234.08	−265.80	−216.80
−0.5	−117.04	−136.08	−103.11
0.5	117.04	106.72	142.43
1.0	234.08	215.01	251.88
1.5	351.10	328.88	347.86
2.0	468.15	424.73	424.73

are applied, similar curves with positive slopes are obtained, which results in the positive electromagnetic stiffness k_v.

3.2. Magnetic stiffness due to the interaction between the PM and the Core

The orthorhombic PM with a dimension of $l \times w \times h$ can be represented by two rectangles of surface pole density $\sigma = \pm M$ [20]. The flux density on the central axis at a distance z from the PM can be calculated as

$$B_z = \frac{\mu_0 M}{\pi}\left[\sin^{-1}\frac{lw}{\sqrt{(l^2+4z^2)(w^2+4z^2)}} - \sin^{-1}\frac{lw}{\sqrt{[l^2+4(z+h)^2][w^2+4(z+h)^2]}}\right]. \tag{12}$$

As many factors affect the production of PMs, their magnetic properties may vary. The Magnetic Materials Producers Association (MMPA) allows for up to 20% variation in magnetic energy from the published values for a grade of magnetic material, this large swing in magnetic properties can greatly affect the performance of any device using PMs. Because of this, the properties of a permanent magnet are normally determined experimentally. In order to identify the magnetization M, the magnetic flux density was measured by using the DC magnetometer at the points off the pole face and along the centerline of the PM. Comparing them with that obtained by Eq. (12), M was found to be $395.8\,\mathrm{kA\,m^{-1}}$. Fig. 9 shows a comparison of the measured values and the computed ones using Eq. (12) with $M = 395.8\,\mathrm{kA\,m^{-1}}$.

To understand the interaction force between the PM and the core, first consider the force between a PM and one end of a ferromagnetic cylinder. This force may be approximated as [21]

$$F = \alpha B_S^2 A, \tag{13}$$

where α is a constant to be determined, A, is the area of the PM surface, and B_S, is the flux density at the surface of the ferromagnetic cylinder. Let F_1 be the interaction force between the right end of the core and the PM and F_2 the interaction force between the left end of the core and the PM (refer to Fig. 3). When the PM is located at the exact middle of the air gap of the core, $F_1 = -F_2$, such that the net force is zero. When the PM is moved to the right, $|F_1| > |F_2|$, and vice versa. Using Eq. (13), the net force acting on the PM is given by

$$F = F_1 - F_2 = \alpha A(B_{S1}^2 - B_{S2}^2), \tag{14}$$

where B_{S1} and B_{S2} are the flux densities at the right and left end of the core, respectively. Considering the fact that the magnetization in the ferromagnetic core induced by the magnetic field of the PM is not uniform and the core is curved, an experiment was set up to determine the relationship of the interaction force and the displacement [22]. Fig. 10 compares the measured forces and the ones obtained using Eq. (14) with $\alpha = 0.913 \times 10^6\,\mathrm{mH^{-1}}$ which was determined by curve-fitting Eq. (14) to the measured values. It can be seen that when the displacement of the PM center is within the range $[-0.005, 0.005]$ m, the interaction force varies

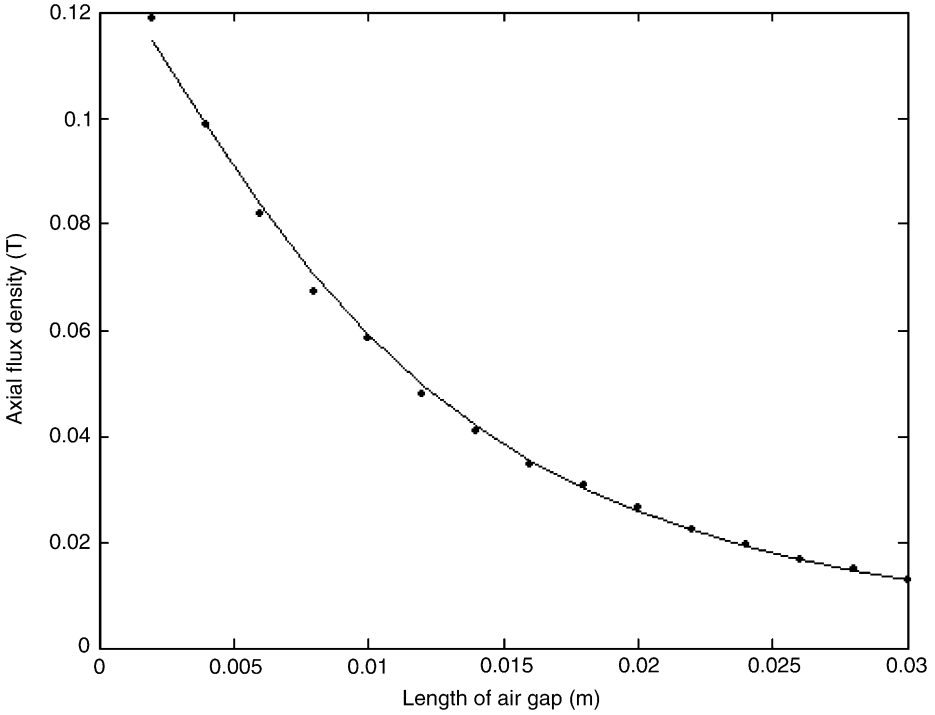

Fig. 9. Flux density B_z at the points along the centerline of the PM with the origin located at the center of the pole face: dot, experimental; solid line, analytical.

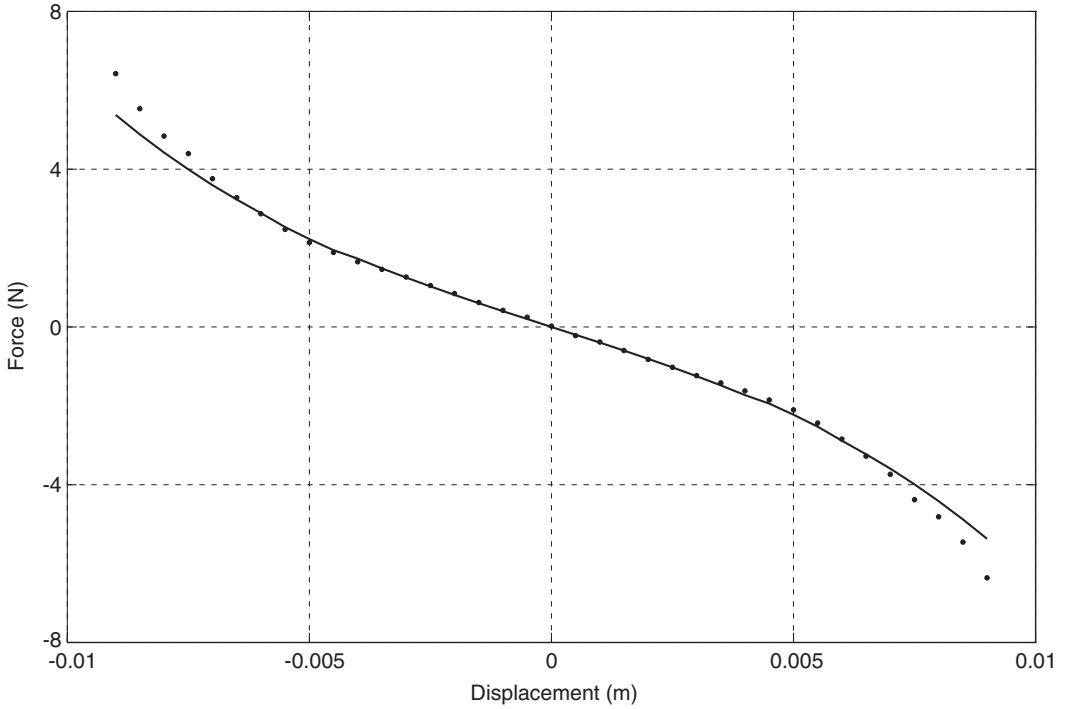

Fig. 10. Interaction force of the PM and the core: dot, experimental; solid line, analytical.

linearly with the change of the displacement, and has a tendency to pull the PM towards the core. Therefore this stiffness k_{c2} is approximated as a constant value of $-417\,\mathrm{N/m}$.

4. Experiment

An experiment was carried out to serve three purposes: initial testing of the absorber system and the entire system, experimental determination of the relationship between the coil current and the absorber natural frequency, and evaluation of the effectiveness of the EMVA in the vibration suppression.

4.1. Preliminary testing

By impact testing, the natural frequency of the primary system was found to be $f_p = 16.0\,\mathrm{Hz}$. In order to prevent resonance, the absorber frequency must be tuned to $f_a = 16.0\,\mathrm{Hz}$ when no current is applied to the electromagnet coils. To achieve it, k_{c1} was adjusted by manually tensioning the absorber beam such that $f_a = 18.1\,\mathrm{Hz}$ without the electromagnet in place. After the electromagnet was installed and k_{c2} took effect, the absorber frequency became 16.0 Hz.

To determine experimentally the magnetic stiffness k_v, the absorber natural frequencies, corresponding to the different coil currents, were found by impact testing. The primary mass was fastened firmly on the ground through a rigid support. The current to the electromagnet was increased from 0 to 2.3 A at a step of 0.1 A, then decreased to -2.3 A at the same step size. Finally the current was loaded up from -2.3 A to 2.3 A at the same pace. For each given current, the absorber mass was tapped and the acceleration signals of the absorber mass were recorded. By applying the fast Fourier transform (FFT) to the measured response, the natural frequency f_a of the absorber was found. Fig. 11 shows the curves of the absorber frequency f_a versus the loading and unloading of the coil current. It exhibits the characteristic of slight hysteresis due to the nature of the steel core. A comparison of the variable stiffness k_v obtained analytically and experimentally is given in Table 2; it indicates that the analytical characterization agrees well with the experimental calibration. The constitutive

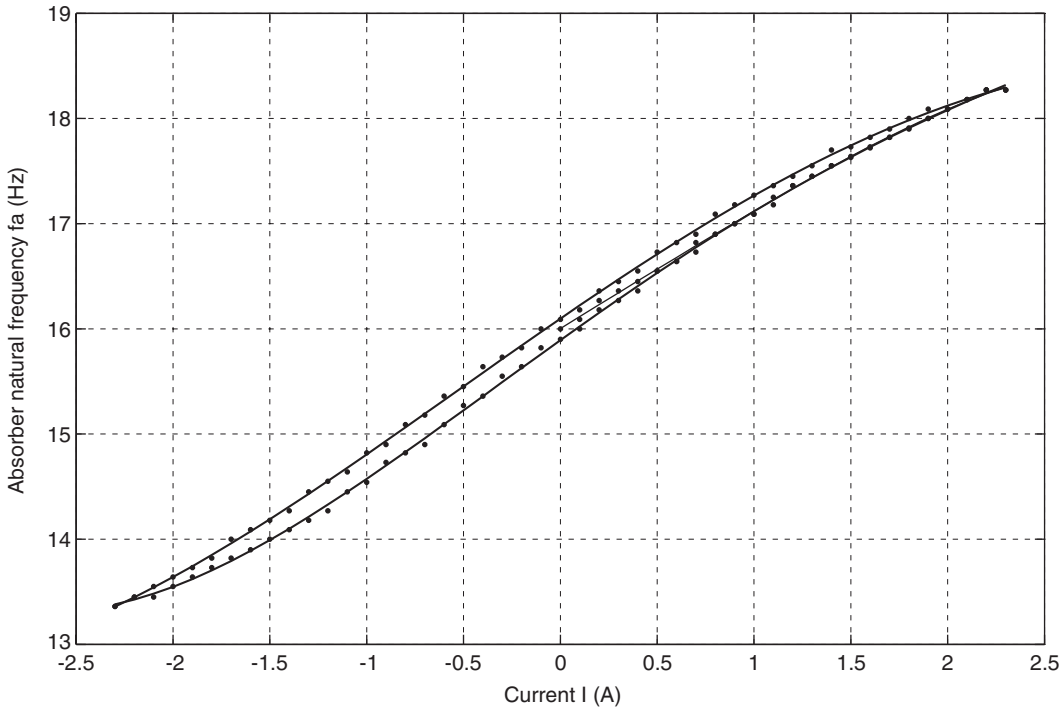

Fig. 11. Absorber frequency versus the coil current during the loading and unloading periods.

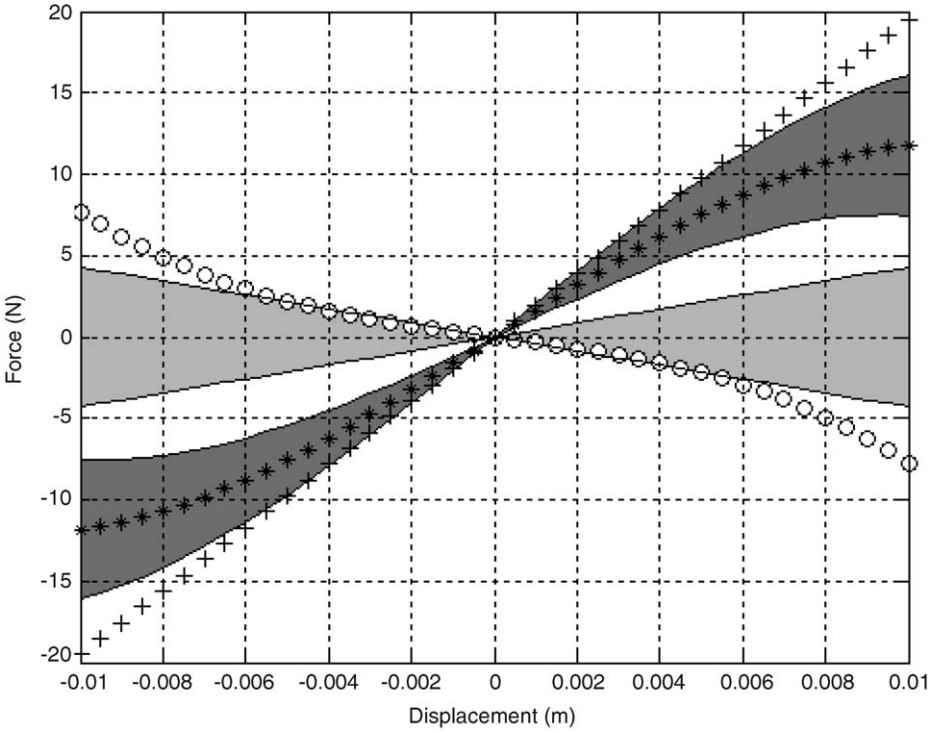

Fig. 12. Constitutive components of the spring forces of the EMVA: plus, force associated with k_{c1}; circle, force associated with k_{c2}; star, force associated with k_c; gray area, adjustable margin for k_v; dark area, adjustable margin for k_a.

components of the spring forces of the entire EMVA are illustrated in Fig. 12, and it also shows the adjustable margin for k_v and the resulting adjustable range for k_a.

To find the relationship between the steady response of the entire system and the exciting frequency, the primary mass was excited by the shaker with a sinusoidal current. The frequency of the sinusoidal signal was swept from 13 to 19.2 Hz at a step of 0.2 Hz; for each step, the steady-state amplitude of the acceleration signal was measured. The curve for the magnitude of the acceleration signals versus the driving frequency was plotted in Fig. 13. It shows that the resonance frequencies of the entire system are 14.5 and 17.9 Hz, respectively, and that the magnitude reaches its lowest point at 16.0 Hz, the anti-resonance frequency.

4.2. Application of the EMVA

The control strategy originates from the traditional design of the passive vibration absorbers. In the case that the system damping is low, the passive vibration absorber can eliminate the vibrations of the primary mass at the design frequency, however, once the exciting frequency shifts away, the primary system may experience severe oscillations. Instead, the tunable EMVA can correspondingly change its frequency to follow the variation of the exciting frequency; as a result, the vibrations of the primary system are effectively suppressed.

As shown in Fig. 14, the governing equations of the dynamics of the 2 dof system with variable stiffness k_v are given by

$$\begin{bmatrix} m & 0 \\ 0 & m_a \end{bmatrix} \begin{bmatrix} \ddot{x}(t) \\ \ddot{x}_a(t) \end{bmatrix} + \begin{bmatrix} c + c_a & -c_a \\ -c_a & c_a \end{bmatrix} \begin{bmatrix} \dot{x}(t) \\ \dot{x}_a(t) \end{bmatrix} + \begin{bmatrix} k + k_a & -k_a \\ -k_a & k_a \end{bmatrix} \begin{bmatrix} x(t) \\ x_a(t) \end{bmatrix} = \begin{bmatrix} F_0 \sin(\omega t) \\ 0 \end{bmatrix},$$

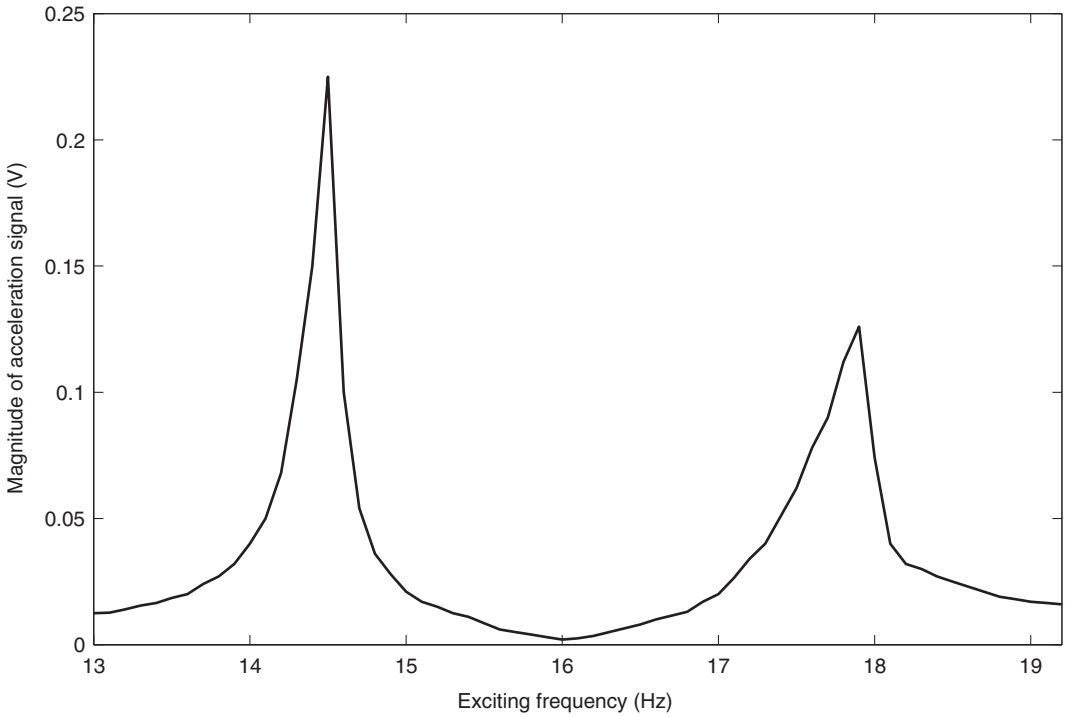

Fig. 13. Magnitude of the acceleration signals versus the driving frequency.

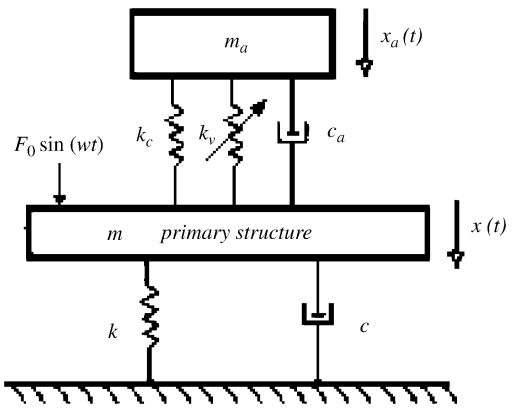

Fig. 14. 2 dof system with variable stiffness k_v.

where $F_0 \sin(\omega t)$ is the external sinusoidal force and $k_a = k_c + k_v$. A mathematical manipulation leads to the steady-state displacement of the primary mass,

$$X = \frac{k_a - m_a\omega^2 + \mathrm{j}c_a\omega}{\begin{vmatrix} k + k_a - m\omega^2 + \mathrm{j}(c + c_a)\omega & -k_a - \mathrm{j}c_a\omega \\ -k_a - \mathrm{j}c_a\omega & k_a - m_a\omega^2 + \mathrm{j}c_a\omega \end{vmatrix}} F_0, \tag{15}$$

where $\mathrm{j} = \sqrt{-1}$. The EMVA may introduce a small damping c_a into the system, which makes impossible the complete elimination of the steady-state vibration of the primary structure; however, the main concern should

be given to the term $k_a - m_a\omega^2$ in the numerator of Eq. (15). Thus the tuning condition is given as

$$\omega_a = \sqrt{\frac{k_c + k_v}{m_a}} = \omega. \tag{16}$$

The objective of the auto-tuning strategy is to ensure that the natural frequency of the absorber equals the exciting frequency, i.e., $f_a = f$, through adjusting the current of the electromagnet. The excitation frequency can be detected by performing FFT on the recorded response of the absorber mass, and the frequency corresponding to the maximum peak of the spectrum of the response is regarded as f. The relationship between the current and the absorber frequency was obtained by conducting a third-order polynomial least-squares curve-fitting using the averaged points of the loading and unloading curves. Fig. 15 shows the averaged points and the best-fit curve. The best-fit curve equation is given as

$$I = -117.3428 + 21.0199 f_a - 1.2995445 f_a^2 + 0.0277619 f_a^3. \tag{17}$$

As depicted in Fig. 2, the response of the absorber mass is measured by an accelerometer (B&K 4393 V), and conditioned via a charger amplifier (B&K Nexus2692). Subsequently, the Data Acquisition Board DS1102 (dSpace) is utilized to convert the signals from analog to digital or digital to analog. ControlDesk (dSpace) provides the interface between Matlab, Simulink and DS1102. A Simulink model was developed to implement on-line tuning. The sampled data are first stored in an S-function named "Buffer" until a specified data length such as $N = 1024$ or 2048 is reached. Then the data are passed to an S function named "FFT" where FFT is conducted and the peak frequency in the FFT spectrum is determined. In the following step, the desired coil current is computed by Eq. (17) and sent to a current regulator board. The output of the board supplies the desired amplitude of the direct current to the electromagnetic coils. The exciting signal is generated by a subsystem within the Simulink model and sent to a power amplifier (B&K 2706). The output of the amplifier drives the electromagnetic shaker to excite the primary system.

Two testing scenarios were devised to test the effectiveness of the EMVA in dealing with variable exciting frequencies: multi-step change and linear change. The multi-step change is composed of three step changes of

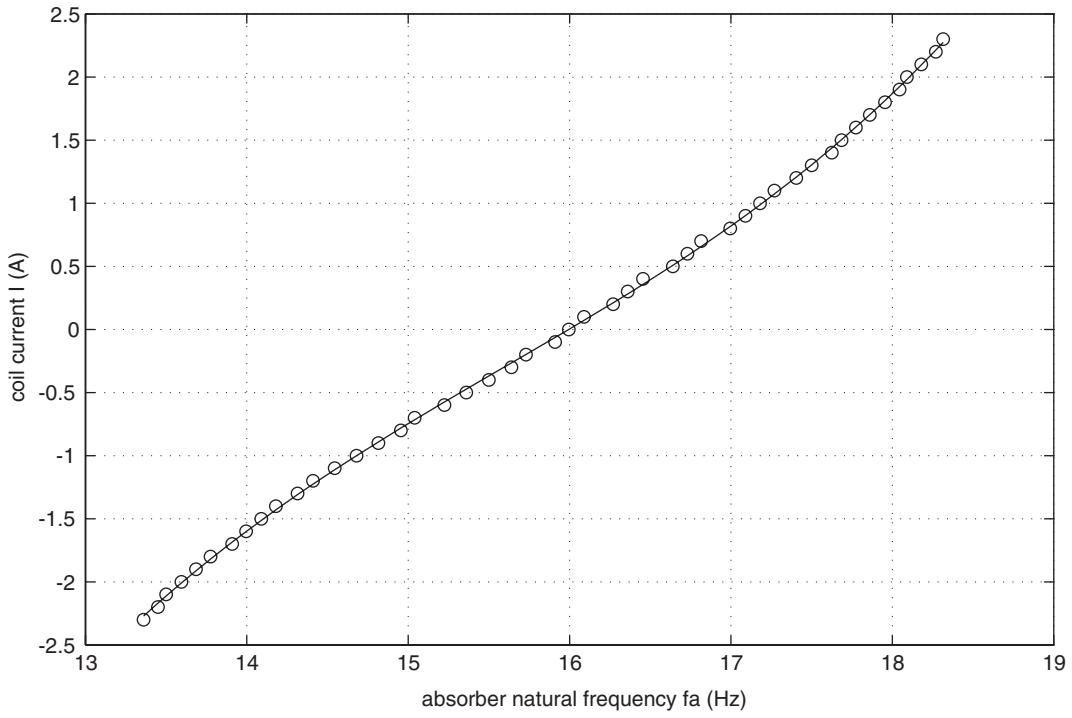

Fig. 15. Relationship between the coil current and the absorber natural frequency: circle, experimental; line, the best-fit curve.

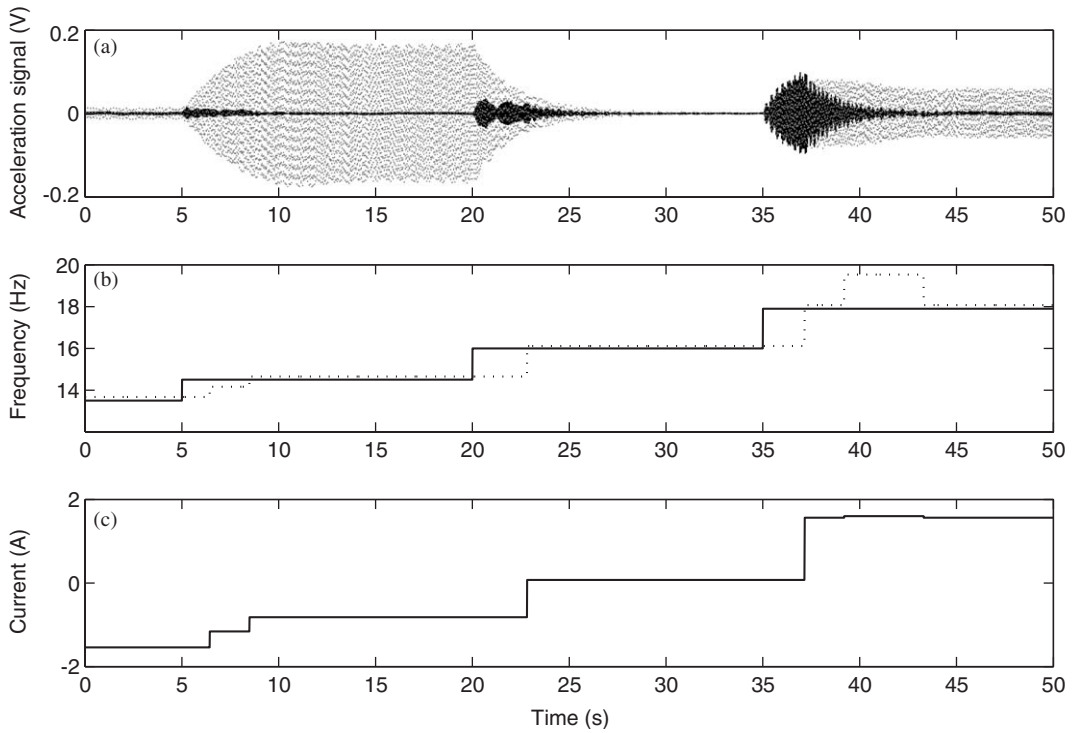

Fig. 16. Experimental results for the multi step change: (a) responses of the primary mass with the untuned EMVA (gray line) or with the tuned EMVA (dark line); (b) the exciting frequency (solid line) and the measured frequency (dotted line); (c) coil current.

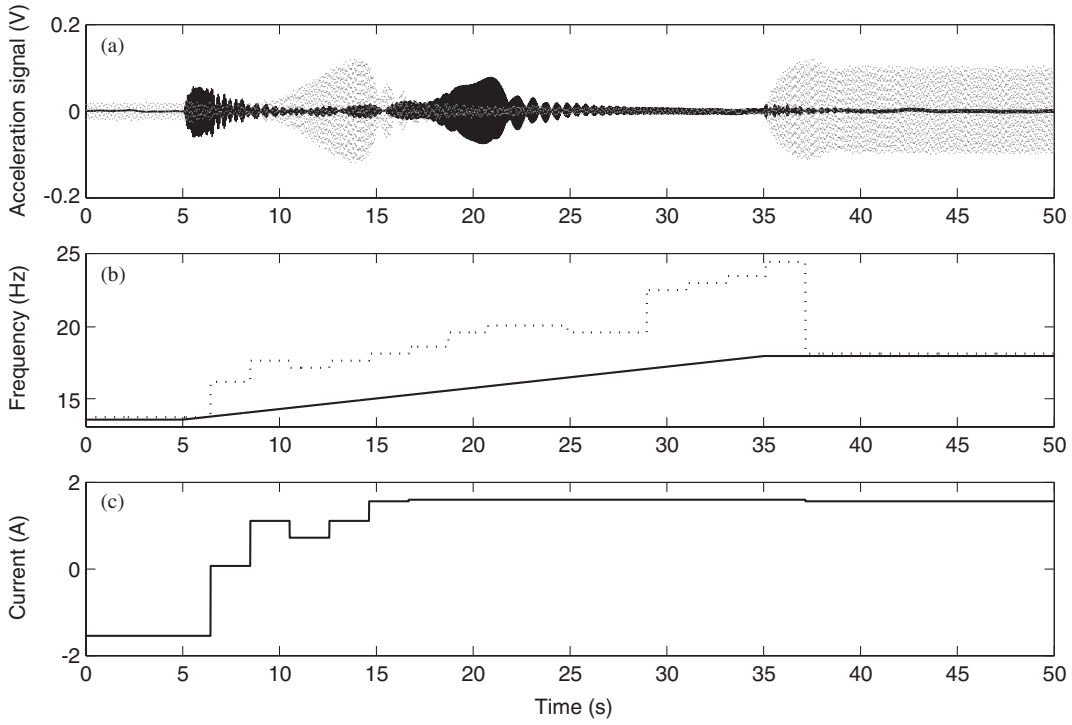

Fig. 17. Experimental results for the linear change: (a) response of the primary mass with the untuned EMVA (gray line) or with the tuned EMVA (dark line); (b) the exciting frequency (solid line) and the measured frequency (dotted line); (c) coil current.

the exciting frequency. For the period of $t<5$ s, the exciting frequency was 13.5 Hz. At $t = 5$ s, the exciting frequency was suddenly changed to 14.5 Hz. At $t = 20$ s, it was changed to 16.0 Hz. At $t = 35$ s, it was changed to 17.9 Hz. Fig. 16 shows the experimental results. When the EMVA was not tuned, the absorber frequency was 16.0 Hz. The first step change brought the system into resonance and the response was increased significantly. The second step change resulted in the anti-resonance and the response was decreased. The third step change once again forced the system into resonance and the response saw another surge. When the auto-tuning control was activated, the EMVA was capable of adjusting its stiffness such that vibration of the primary mass was promptly suppressed at each stage. As the data length used was $N = 2048$, the reaction time for tuning was 2.048 s. It should be noted that the reaction time is solely dependent on the tuning algorithm, while for those motor-driven devices [1–5] extra time is needed for the desired stiffness to be reached. For the linear change, the exciting frequency was varied linearly from 13.5 to 17.9 Hz. Fig. 17 shows the results. It is noted that the tuning algorithm based on FFT failed to follow the variation of the exciting frequency. When the exciting frequency was continuously changed, the transient responses were excited out such that the response was dominated by a component associated with one of the natural frequencies. The peak frequency in the FFT spectrum corresponded to the natural frequency instead of the exciting frequency. Such a limitation of the FFT-based algorithm was addressed in Ref. [5].

5. Conclusion

An electromagnetic vibration absorber (EMVA) has been developed. By varying the current to the electromagnet, the absorber stiffness can be on-line adjusted; as a result, it can cope with a harmonic excitation with a variable frequency. A stiffness characterization has been presented. The fundamental theory of electromagnetism has been employed to establish the analytical relation for the variable magnetic stiffness. The analytical relation has been validated experimentally. The effectiveness of the electromagnetic vibration absorber has been tested. The experiment has shown that the EMVA is capable of adjusting its frequency such that the tuning condition is satisfied in the event of variation of the exciting frequency. The main advantages of the proposed device lie in its rapid reaction and motionless adjustment. The analytical approaches employed in this study are useful for further optimization of the device and for the design of any new devices involved in similar applications of electromagnetism.

Several aspects deserve further discussion. The EMVA is capable of adjusting its stiffness instantaneously. A choice of switching time may affect the transients. It is well known that for free response of a simple spring–mass system, if the spring stiffness is changed from a low value to a high value at a zero velocity and non-zero displacement, a large transient will be induced. However, the present system is a damped 2 dof one, subjected to an external excitation: the relationship between the transients and a switching time is more complicated than that for an undamped 1 dof system. In the experiment, no significant transients were observed when different switching times were tried. As well, the main concern of the study is suppression of the steady-state response. The transient responses will die out as the system possesses a certain degree of damping. Minimization of energy consumption remains for further study. Limited by the budget available, the present design is not an optimum one. It is expected that with an improvement of material selection and fabrication, the device can be made more efficient. As the EMVA has no mechanical drive system, it can easily be miniaturized. This feature may be explored in micro-electro-mechanical systems (MEMS) devices.

Acknowledgments

The authors would like to express their gratitude to the National Science and Engineering Research Council of Canada for financial support. The authors would also like to thank Mr. K. Batia for his help in the fabrication of the experimental apparatus.

References

[1] M.A. Franchek, M.W. Ryan, R.J. Bernhard, Adaptive passive vibration control, *Journal of Sound and Vibration* 189 (1995) 565–585.

[2] C. Buhr, M.A. Franchek, R.J. Bernhard, Non-collocated adaptive-passive vibration control, *Journal of Sound and Vibration* 206 (1997) 371–398.
[3] K. Nagaya, A. Kurusu, S. Ikai, Y. Shitani, Vibration control of a structure by using a tunable absorber and an optimal vibration absorber under auto-tuning control, *Journal of Sound and Vibration* 228 (1999) 773–792.
[4] N. Varadarajan and S. Nagarajaiah, Response control of building with variable stiffness tuned mass damper using empirical mode decomposition and Hilbert transform algorithm, *16th ASCE Engineering Mechanics Conference*, July 2003, Seattle.
[5] K. Liu, L. Liao, J. Liu, Comparison of two auto-tuning methods for a variable stiffness vibration absorber, *The Transactions of Canadian Society for Mechanical Engineering* 29 (2005) 81–96.
[6] W.N. Patten, R.L. Sack, Q. He, Controlled semiactive hydraulic vibration absorber for bridges, *Journal of Structural Engineering* 122 (1996) 187–192.
[7] M.D. Symans, M.C. Constantinou, Seismic testing of a building structure with a semi-active fluid damper control system, *Earthquake Engineering and Structural Dynamics* 26 (1997) 759–777.
[8] P. Dupont, P. Kasturi, A. Stokes, Semi-active control of friction dampers, *Journal of Sound and Vibration* 202 (1997) 203–218.
[9] L.Y. Lu, Semi-active modal control seismic structures with variable friction dampers, *Engineering Structures* 26 (2004) 437–454.
[10] S.B. Choi, H.K. Lee, E.G. Chang, Field test results of a semi-active ER suspension system associated with skyhook controller, *Mechatronics* 11 (2001) 345–353.
[11] A. Milecki, Investigation and control of magneto-rehological fluid dampers, *International Journal of Machine Tools & Manufacture* 41 (2001) 379–391.
[12] B. Erkus, M. Abe, Y. Fujino, Investigation of semi-active control for seismic protection of elevated highway bridges, *Engineering Structures* 24 (2002) 281–293.
[13] T. Mizuno, K. Araki, Control system design of a dynamic vibration absorber with an electromagnetic servomechanism, *Mechanical Systems and Signal Processing* 7 (1993) 293–306.
[14] M.S. Trimboli, R. Wimmel, E. Breitbach, A quasi-active approach to vibration isolation using magnetic springs, *SPIE* 2193 (1994) 73–83.
[15] Y. Matsuzaki, T. Ikeda, A. Nae, T. Sasaki, Electromagnetic forces for a new vibration control system: experimental verification, *Smart Materials and Structures* 9 (2000) 127–131.
[16] C.C. Chen, M.K. Yeh, Parametric instability of a beam under electromagnetic excitation, *Journal of Sound and Vibration* 240 (2001) 747–764.
[17] S. Yashita and K. Seto, Vibration and noise control using dual dynamic absorbers with magnetic damping, *Proceedings of The Third International ISEM Symposium on the Application of Electromagnetic Forces*, Sendai, 1992.
[18] D. Kienholz, S. Pendleton, Demonstration of solar array vibration suppression, *SPIE* 2193 (1994) 59–72.
[19] K. Liu, J. Liu, L. Liao, Application of a tunable electromagnetic damper in suppression of structural vibration, *The Transactions of the Canadian Society for Mechanical Engineering*, February 2006 (in press).
[20] D.J. Craik, *Magnetism: Principles and Applications*, Wiley, Chichester, New York, 1995.
[21] H.H. Woodson, J.R. Melcher, *Electromechanical Dynamics—part I: Discrete Systems*, Wiley, New York, 1968.
[22] J. Liu, Design and Implementation of a Tunable Vibration Absorber and a Time-Delayed Vibration Absorber, MSc Thesis, Lakehead University, Canada, 2005.